nature portfolio

https://doi.org/10.1038/s41561-022-00974-7

Supplementary information

Springtime arctic ozone depletion forces northern hemisphere climate anomalies

In the format provided by the authors and unedited

Springtime arctic ozone depletion forces northern hemisphere climate anomalies - Supplementary Information

Marina Friedel[1,*], Gabriel Chiodo[1], Andrea Stenke[1,2,3], Daniela I.V. Domeisen[4,1], Stephan Fueglistaler[5,6], Julien G. Anet[7], and Thomas Peter[1]

[1]ETH Zürich, Institute for Atmospheric and Climate Science, Zürich, Switzerland
[2]ETH Zürich, Institute of Biogeochemistry and Pollutant Dynamics, Zürich, Switzerland
[3]Eawag, Swiss Federal Institute of Aquatic Science and Technology, Dübendorf, Switzerland
[4]University of Lausanne, Lausanne, Switzerland
[5]Department of Geosciences, Princeton University, Princeton, NJ, USA
[6]Program in Atmospheric and Oceanic Sciences, Princeton University, Princeton, NJ, USA
[7]ZHAW, School of Engineering, Winterthur, Switzerland
[*]marina.friedel@env.ethz.ch

S1. Further comments on results from SOCOL-MPIOM

In the following, results obtained by the second chemistry-climate model, SOCOL-MPIOM, are discussed. Extended Data Figures 1, 3 and 4 are analogous to Figures 1, 4 and 5 in the main text for SOCOL-MPIOM. Like in WACCM, also with this model the observed surface pattern following spring ozone depletion can be reproduced. The magnitude of the positive Arctic Oscillation (AO) and certain features of the surface signal (like the dry anomaly over Europe) in SOCOL-MPIOM runs without interactive ozone chemistry (CLIM-3D and CLIM-2D) are less pronounced than in simulations including ozone feedback (INT-O3). Overall, Extended Data Figure 2 shows that experiments with a zonal mean ozone forcing (CLIM-2D) on average only capture 30% of the AO signal following strong spring Arctic ozone depletion, while simulations with a three-dimensional ozone forcing reproduce 60% of the AO signal. The magnitude of the AO response is thus model-dependent (see also Fig. S2), while the sign of the AO change after the ozone minima is robust across models. These results show that also in SOCOL-MPIOM, which has a different dynamical core and chemistry module compared to WACCM, ozone feedbacks play an important role in shaping spring NH surface climate, albeit with a slightly smaller signal (Figs. 1, Extended Data Figures 1, 2).

Compared to WACCM, ozone asymmetries play a more important role in SOCOL-MPIOM. Applying a three-dimensional ozone forcing as in CLIM-3D improves the surface signal compared to a zonal mean ozone forcing (as in CLIM-2D) significantly in SOCOL-MPIOM. This is related to an overestimated asymmetry of the ozone field in SOCOL-MPIOM, as shown in Figure S3 and discussed in section S3. However, also in this model, ozone feedbacks are important in order to reproduce the full magnitude and certain details of the surface pattern (like the increased dry conditions over Europe after ozone depletion as well as the negative SLP over the pole).

As in WACCM, the larger surface signal in INT-3D in SOCOL-MPIOM can be linked to stronger and more persistent cold anomalies in the lower stratosphere and a stronger stratosphere-troposphere coupling in the aftermath of ozone depletion (Extended Data Figure 3). Both models show prolonged winter conditions in the lower stratosphere in INT-3D compared to CLIM experiments. Moreover, the dynamical heating (see equation (2) in the methods section) in the middle stratosphere after day 30, which leads to warm anomalies in INT-3D in the middle and upper stratosphere (Extended Data Figure 4 a, b, c, d), is reproduced by both models (Extended Data Figure 4 m, n, o, p) independently of the choice of ozone forcing, which increases our confidence in the ozone feedback mechanism described in the main text. For the CLIM experiments, anomalies in ozone are zero. Thus, plots e-h equal composites of polar cap ozone anomalies in INT-3D around the ozone minimum. Lower stratospheric anomalies in SOCOL-MPIOM are more persistent in INT-3D than in CLIM experiments, albeit less than in WACCM. The tropospheric response is sensitive to the lifetime of stratospheric anomalies[1]. Hence, the shorter-lived NAM anomalies in the lower stratosphere in SOCOL-MPIOM may explain the smaller surface AO response in this model compared to WACCM.

S2. Effects of ozone depletion in WACCM and SOCOL-MPIOM

Extended Data Figure 5 shows differences between INT-O3 and both CLIM-3D and CLIM-2D in terms of SLP, surface temperature and precipitation anomalies following spring ozone depletion in WACCM. Extended Data Figure 6 shows differences between INT-3D and CLIM simulations in SOCOL-MPIOM. Differences between INT-3D and CLIM-3D can directly be attributed to ozone feedbacks, differences between INT-3D and CLIM-2D arise from ozone feedbacks and zonal asymmetries in the ozone distribution, which are neglected in CLIM-2D. Differences between INT-3D and CLIM-3D are smaller in both models compared to differences between INT-3D and CLIM-2D. Especially the high pressure anomaly over Europe is better captured when a three-dimensional ozone forcing is applied as in CLIM-3D. However, there are significant differences between INT-3D and CLIM-3D among models, which are forced by ozone feedbacks. Both WACCM and SOCOL-MPIOM simulations show in a robust manner that ozone feedbacks strengthen negative SLP anomalies over the pole and positive SLP anomalies in the midlatitudes (and thus strengthen the positive AO signal). Moreover, both models show that ozone feedbacks force drier conditions over Europe, especially over UK, and more precipitation over Iceland and the west coast of North America.

We test the robustness of the AO response by constructing 5000 synthetic AO differences between INT and CLIM-3D (CLIM-2D) for WACCM and SOCOL-MPIOM, whose distributions are shown in Figure S2. For further information on the bootstrapping method, refer to the methods section ("2-sample bootstrapping significance test"). The actual difference between mean AO values between INT-3D amd CLIM-3D (CLIM-2D) experiments (as shown on Fig. 2, Extended Data Figure 2) is marked in Figure S2 by the red stippled line. The obtained distributions show that the difference in mean in the month after ozone depletion is highly robust in WACCM, where less than 2% of the synthetic AO differences show a larger positive value than for ozone minimum years. For SOCOL-MPIOM, the same tendency can be seen. However, the difference in the mean AO index between INT-3D and CLIM-3D (CLIM-2D) is smaller than in WACCM. In SOCOL-MPIOM, the mean AO index is less representative of the actual surface signal than in WACCM, as the SLP pattern is less congruent with the mean AO index after ozone depletion (see Fig. S1).

Table S1 shows final warming dates in years with ozone depletion in WACCM, SOCOL-MPIOM and MERRA2. Results show that ozone feedbacks during ozone minima extend winter conditions in the stratosphere for up to 10 days.

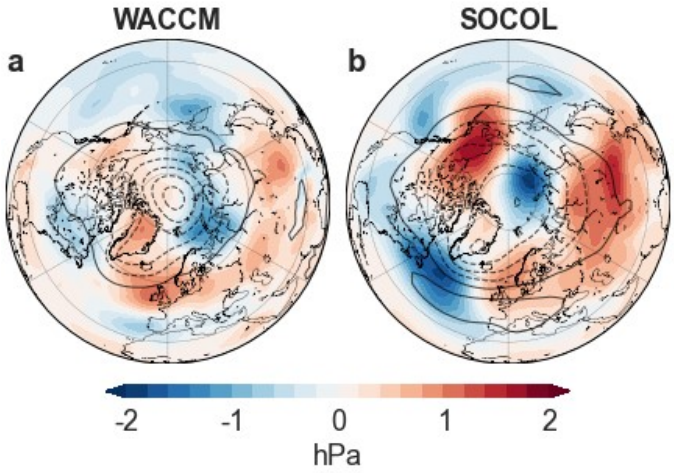

Supplementary Figure S1. Congruence of AO index and sea level pressure anomalies. Differences between the actual SLP anomalies and the SLP anomalies congruent with the mean AO index in the month after the ozone minimum in WACCM INT-3D (a) and SOCOL-MPIOM INT-3D (b). The congruent SLP pattern has been calculated by regressing SLP anomalies onto the AO index for each grid point and multiplying the regression pattern by the mean AO index in the month after the ozone minima (0.50 for WACCM and 0.54 for SOCOL). Black contour lines show the AO regression pattern in units of 2 hPa σ^{-1}.

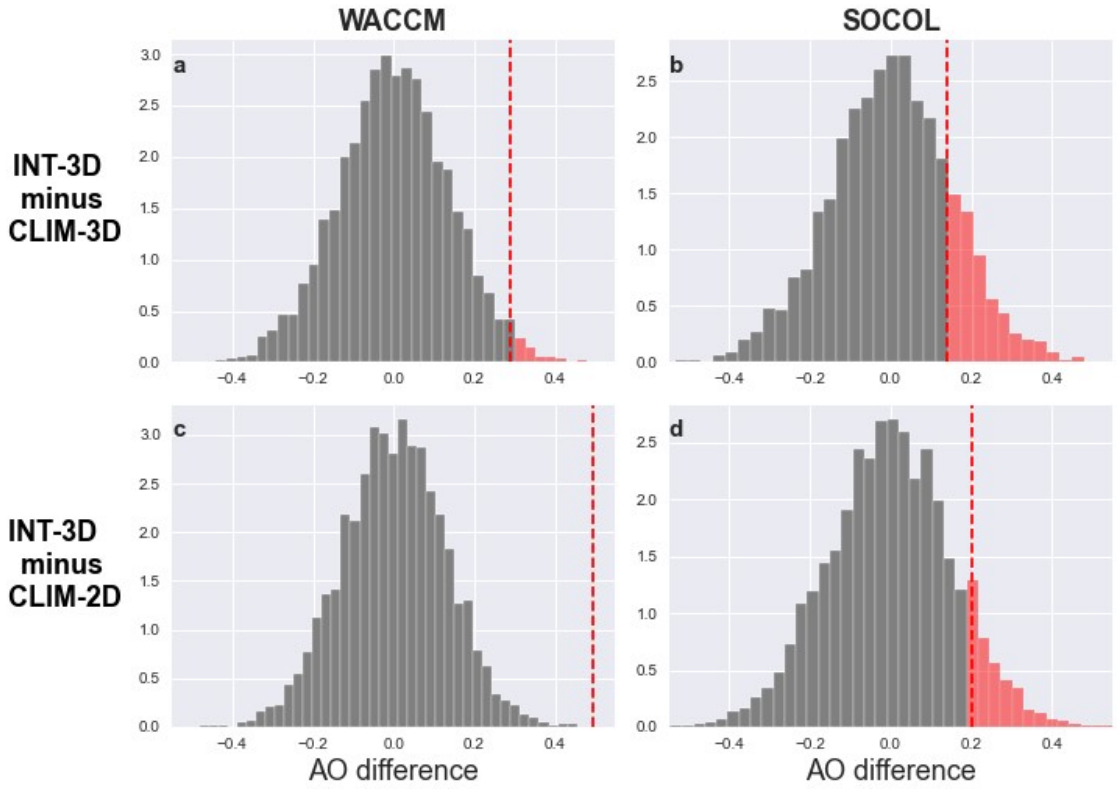

Supplementary Figure S2. Robustness of AO response in WACCM and SOCOL-MPIOM. Distribution of 5000 bootstrapping samples of differences in the AO between WACCM INT-3D minus CLIM-3D (a), WACCM INT-3D minus CLIM-2D (c), SOCOL INT-3D minus CLIM-3D (b) and SOCOL-MPIOM INT-3D minus CLIM-2D (d). The actual mean AO difference between INT-3D and CLIM-3D (CLIM-2D) for ozone minima years is shown by the red stippled line. Red marked parts of the histogram are bootstrapping samples which exceed the AO difference in low ozone years.

	WACCM	SOCOL-MPIOM	MERRA2
INT-3D	9 May	22 April	15 April
CLIM-3D	28 April	10 April	
CLIM-2D	28 April	13 April	

Supplementary Table S1. Final warming dates after ozone depletion. Final warming dates at 10 hPa in WACCM and SOCOL-MPIOM INT-3D, CLIM-3D and CLIM-2D as well as in MERRA2 for the 25% of years with the lowest spring ozone concentrations.

S3. Impact of zonal asymmetries in the climatological ozone forcing

The Arctic stratospheric polar vortex is not symmetric around the pole, but displaced towards Eurasia. Figure S4 shows potential vorticity at 10 hPa as a proxy for the polar vortex strength. In all datasets, the polar vortex displacement towards Eurasia can be seen. This leads to a zonally asymmetric stratospheric ozone distribution with a maximum over the North Pacific. Figure S3 a, b and c shows the ozone climatology (partial ozone column, 30-70 hPa) in March and April in SOCOL-MPIOM INT-3D, WACCM INT-3D and MERRA2. In all models, the ozone field is displaced towards the North Pacific. In SOCOL-MPIOM, both the ozone concentrations as well as the ozone asymmetry are larger than in MERRA2 and WACCM, which is related to a stronger vortex displacement in this model (see Fig. S4). Compared to MERRA2, WACCM underestimates zonal ozone asymmetries, while SOCOL-MPIOM heavily overestimates them.

The middle row in Figure S3 (panels d-f) shows the ozone concentration in WACCM INT-3D, SOCOL-MPIOM INT-3D and MERRA2 compared to their respective zonal mean ozone climatologies around the ozone minimum date. This difference shows the magnitude of the O3 minimum and its displacement compared to a zonal mean climatology, and as such the additional ozone forcing in INT-3D compared to CLIM-2D. The bottom row in Figure S3 (panels g-i) shows the ozone concentration in WACCM INT-3D, SOCOL-MPIOM INT-3D and MERRA2 compared to the three-dimensional ozone climatology of the respective models around the ozone minimum date, which shows the additional ozone forcing in INT-O3 compared to CLIM-3D. It is apparent that SOCOL-MPIOM overestimates the ozone minima in terms of both asymmetry and depth. Especially in SOCOL-MPIOM, differences between INT-3D and CLIM-3D (panel h) are smaller than between INT-3D and CLIM-2D (panel e) in magnitude (more than 10 DU) and location (more symmetric). In both WACCM and MERRA2, differences between the zonal mean and three-dimensional ozone climatologies are smaller than in SOCOL-MPIOM.

Ozone asymmetries lead to an asymmetric heating of the polar stratosphere, causing a further displacement of the polar vortex during strong polar vortex states[2]. We explore the impact of ozone asymmetries on the polar vortex strength and location by analysing anomalies in potential vorticity (PV) following strong ozone depletion. Figure S5 shows the influence of the differences in ozone forcing discussed in Figure S3 on PV anomalies around the ozone minimum. In WACCM (panel a), differences between the interactive (INT-3D) and prescribed climatological ozone simulations are almost identical for both CLIM-3D and CLIM-2D, which means that ozone asymmetries do not impact the strength or location of PV anomalies in WACCM. In SOCOL-MPIOM, however, differences in PV anomalies around the ozone minima between INT-3D and CLIM-3D are smaller than between INT-3D and CLIM-2D. In this model, asymmetries in the ozone climatology do impact the location and strength of the PV anomalies around the ozone minima. This is probably due to the larger zonal ozone asymmetries in the SOCOL-MPIOM ozone climatology compared to WACCM (Fig. S8).

In models with strong asymmetric ozone distributions, like in SOCOL-MPIOM, simulations with a three-dimensional ozone forcing thus better represent the Arctic polar vortex during ozone depletion conditions (Fig. S8 e, h). In models where ozone asymmetries are small, like in WACCM, a three-dimensional ozone forcing does not show such improvements (Fig. S8 d, g). The impact of zonal asymmetries of a climatological ozone forcing is thus model dependent. However, the magnitude of the strong polar vortex anomaly and its displacement can only be fully captured in simulations with interactive ozone chemistry in both models (see remaining differences between INT-O3 and CLIM-3D in Fig. S5 d and e).

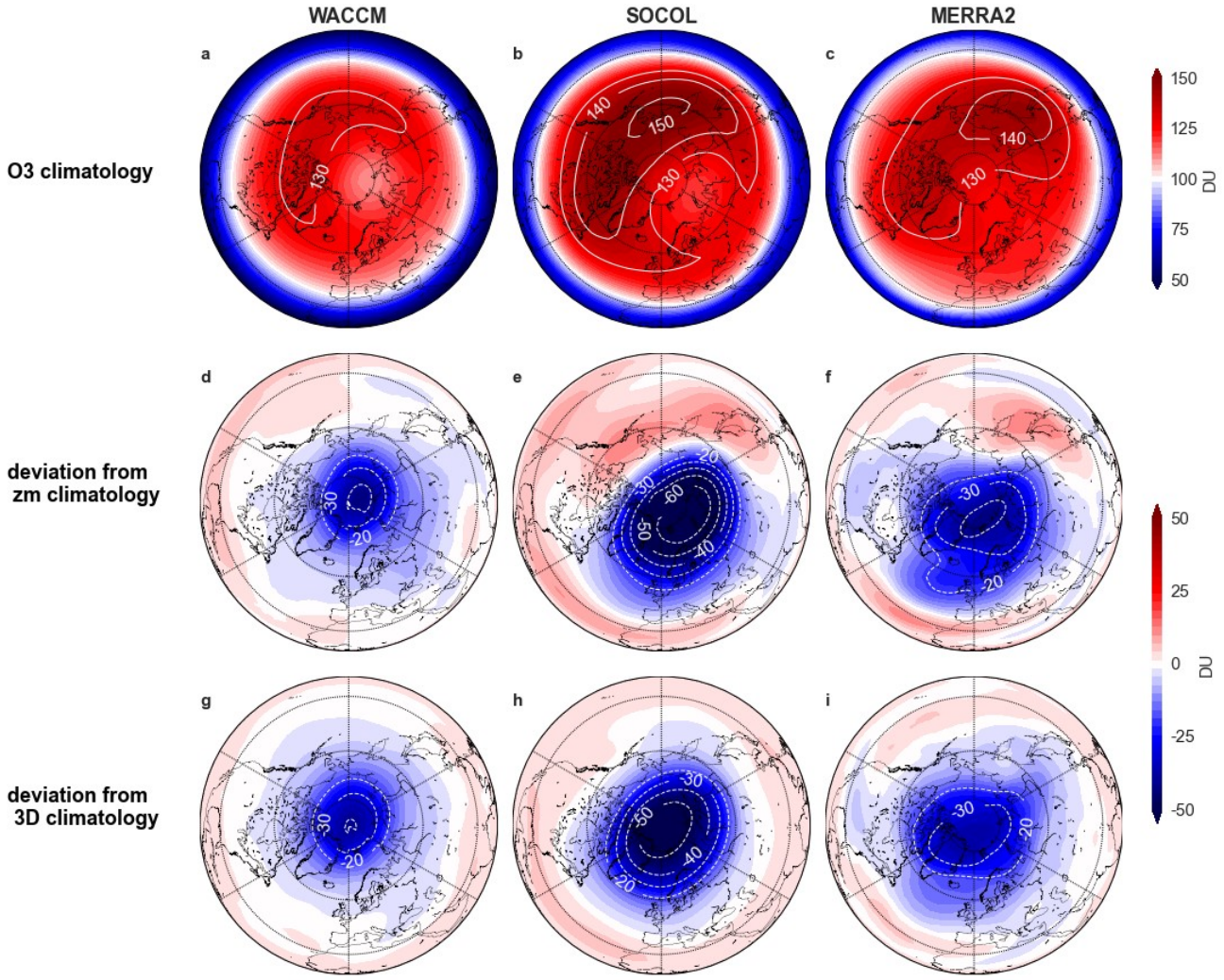

Supplementary Figure S3. Ozone forcing. Ozone climatology in March and April (partial ozone column 30-70 hPa) in WACCM INT-3D (a), SOCOL-MPIOM INT-3D (b) and MERRA2 (c) as well as deviations of partial ozone column (30-70 hPa) in the 30 days after the ozone minimum date from the zonal mean ozone climatology (d-f) and the three-dimensional ozone climatology (g-i) of the respective model.

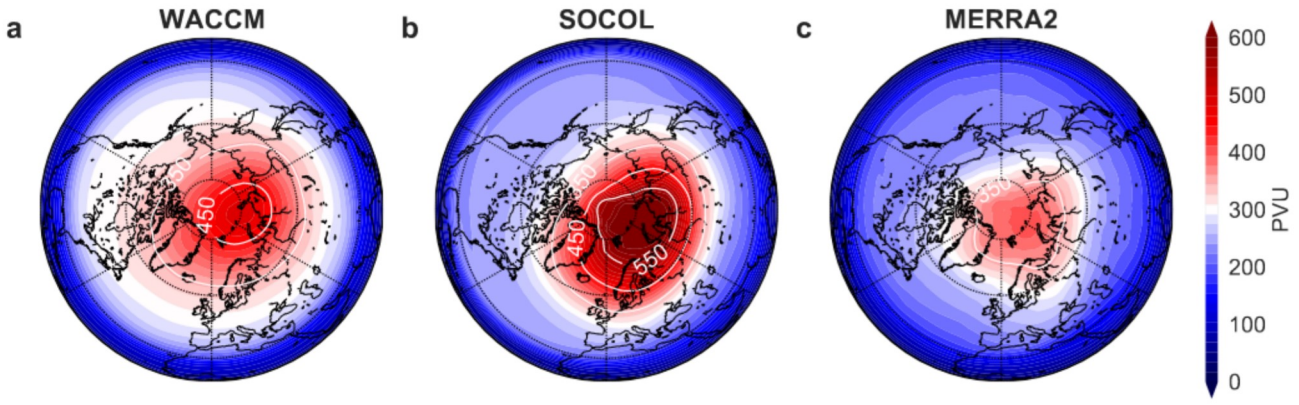

Supplementary Figure S4. Potential Vorticity at 10 hPa after ozone depletion. Absolute potential vorticity (PV) following ozone minima in WACCM INT-3D (a), SOCOL-MPIOM INT-3D (b) and MERRA2 (c) (average over the 30 days after the ozone minimum date in the 25% of years with the lowest spring ozone concentrations).

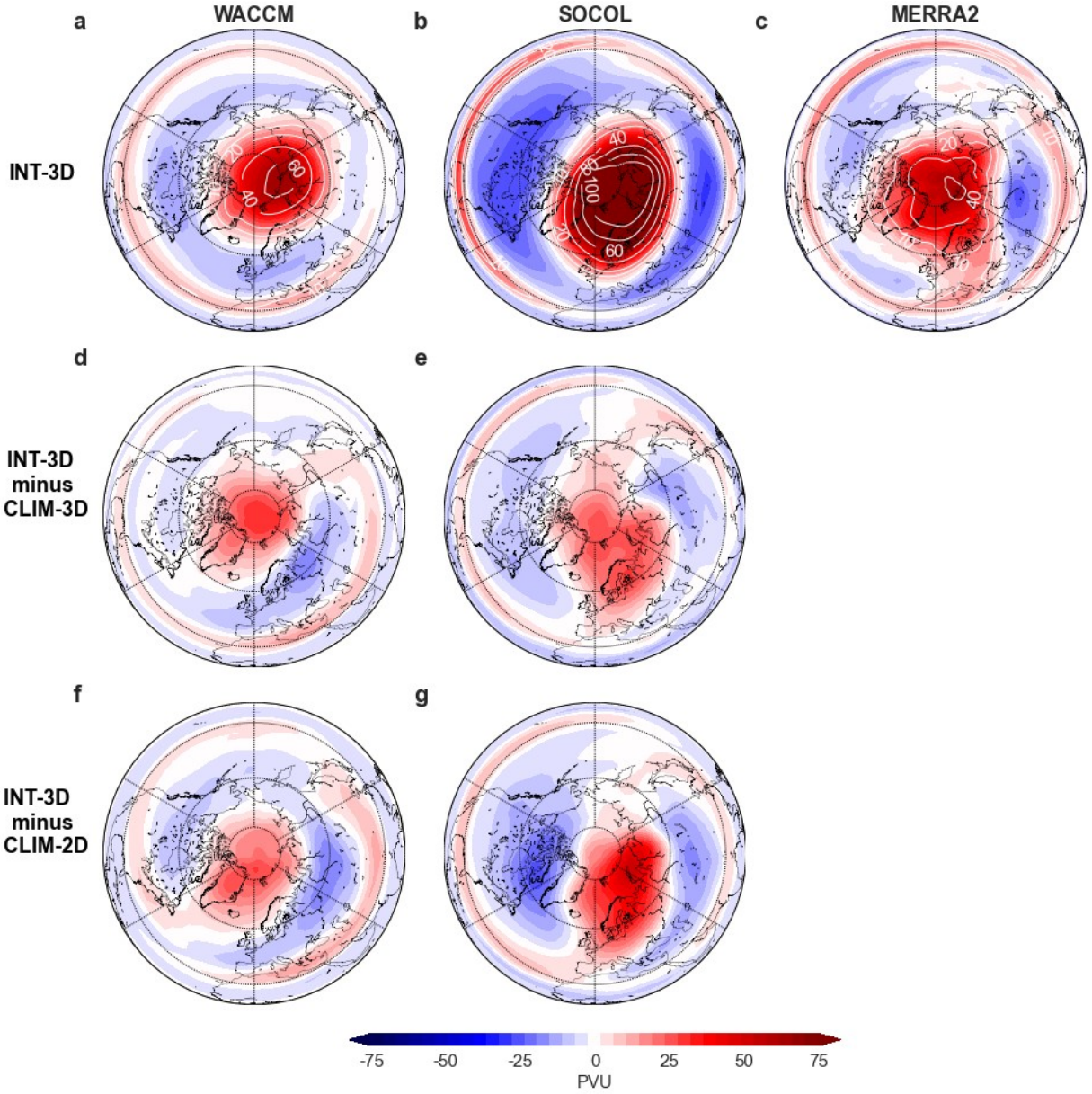

Supplementary Figure S5. Anomalies in Potential Vorticity. PV anomalies at 10 hPa around the ozone minimum date (days -5 - 5) in the 25% of years with the lowest spring ozone concentrations at 10 hPa in WACCM (a), SOCOL-MPIOM (b) and MERRA2 (c). Differences in PV anomalies around the ozone minimum between INT-3D and CLIM-3D (d, e) as well as between INT-3D and CLIM-2D (f, g).

S4. Additional notes on methods

All model simulations performed for this study are listed in table S2. All model simulations apply present-day (year-2000) boundary conditions. The integrations are branched off historical interactive simulations. As such, the model is not in perfect equilibrium, but shows very small trends due to the inertia of the ocean (generally smaller than 0.1 K per century in WACCM, and 0.2-0.3 K per century in SOCOL-MPIOM), as seen in Figure S6. Note that these trends are negligible compared to the large interannual variability of the variables of interest. No trends can be seen in the spring AO indices, neither in the models nor the observations (not shown).

Figure S7 shows the ozone standard deviation in spring in the two chemistry-climate models WACCM and SOCOL-MPIOM as well as in the observations, and Figure S8 shows the evolution of ozone minima (blue lines). WACCM and SOCOL-MPIOM differ in the magnitude and timing of the maximum ozone variability in spring: Ozone minima in WACCM are more predominantly located in the upper stratosphere compared to SOCOL-MPIOM and are in general less pronounced. This is probably due to the smaller chemical contribution to the ozone minima in WACCM compared to SOCOL-MPIOM (see Fig. S10 and pertaining discussion in section S5).

Figure S9 shows a comparison of the ozone depletion detection method used in this study based on daily ozone values (Fig. S9 a), and the detection method used in earlier studies based on a fixed reference month in MERRA2 (March, Fig. S9 b), e.g.[3,4]. The surface signal in the aftermath of springtime ozone depletion found with the new detection method, which takes inter-annual variations in the timing of those events into account, is stronger for a large part of the Northern Hemisphere.

Name	Model	O3 Forcing	Ensemble Members	Years
INT-3D	WACCM	interactive	1	200
CLIM-3D	WACCM	3D climatology from INT-3D (WACCM)	2	200 (100, 100)
CLIM-2D	WACCM	zonal mean climatology from INT-3D (WACCM)	2	200 (100, 100)
INT-3D	SOCOL-MPIOM	interactive	3	200 (99, 98, 3)
CLIM-3D	SOCOL-MPIOM	3D climatology from INT-3D (SOCOL)	3	200 (95, 95, 10)
CLIM-2D	SOCOL-MPIOM	zonal mean climatology from INT-3D (SOCOL)	3	200 (97, 97, 6)

Supplementary Table S2. Summary of all model simulations conducted for this study. Some simulations are composed of 2-3 ensemble members with a total of 200 years.

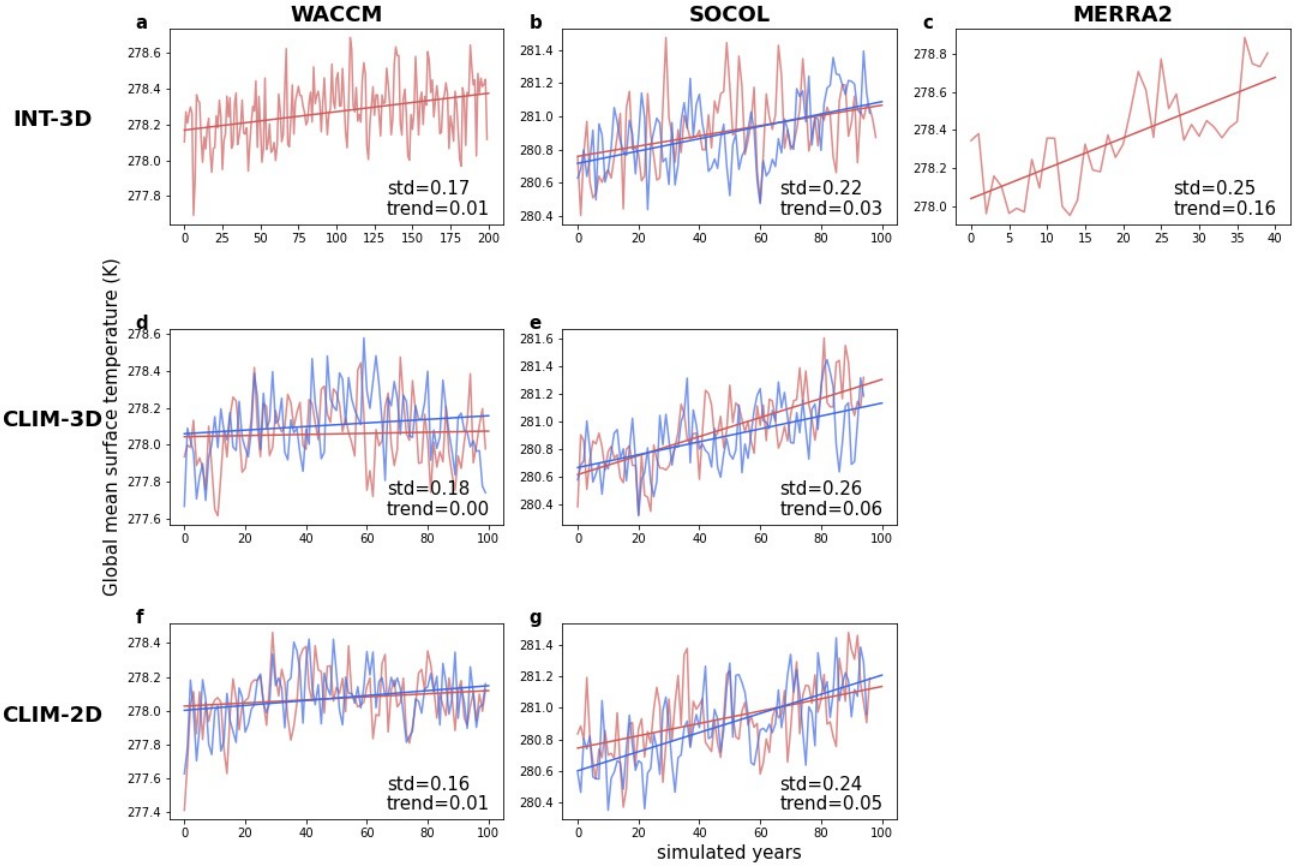

Supplementary Figure S6. Trends in global mean surface temperature. Yearly, global mean surface temperature as well as a linear fit in WACCM (left column), SOCOL-MPIOM (second column) and MERRA2 (right column). Different ensemble members are shown in red and blue, respectively. Shown are also values for the standard deviation of yearly mean, global mean surface temperature (in K) as well as its trend (in K/decade) averaged over ensemble members.

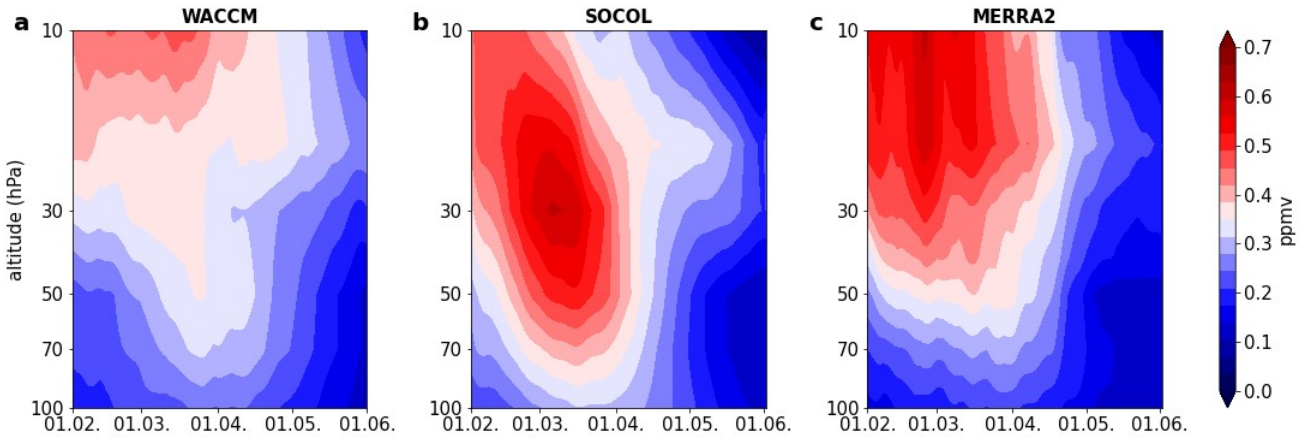

Supplementary Figure S7. Interannual ozone variability. Ozone standard deviation in spring in WACCM (INT-3D) (a), SOCOL-MPIOM (INT-3D) (b) and MERRA2 (c). Since the altitude of maximum ozone variance differs between datasets, partial ozone column between 30-70 hPa was chosen to define ozone minima.

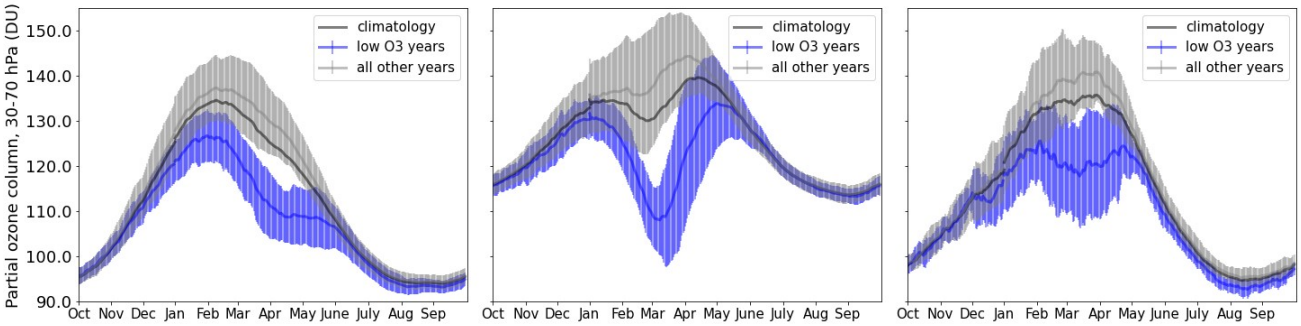

Supplementary Figure S8. Mean ozone evolution in years with ozone depletion. Mean ozone evolution at 30-70 hPa with standard deviation (shading) for INT-3D from WACCM (a), SOCOL-MPIOM (b) and MERRA2 (c) (in Dobson Units (DU)). Blue lines show the 25% of years with lowest ozone values in spring (March – April), grey lines show all other 75% of years. The black line shows the daily mean ozone climatology derived from INT-3D, which is used as ozone forcing in CLIM-3D runs. WACCM and SOCOL-MPIOM records are 200 years long each, the MERRA2 record contains 41 years.

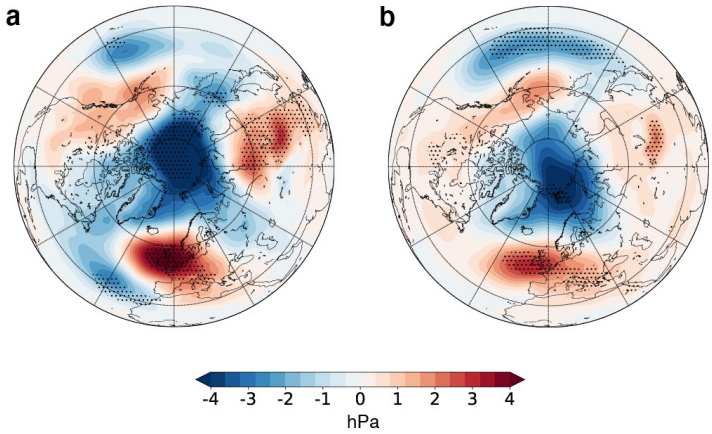

Supplementary Figure S9. Impact of new detection method. Comparison of ozone depletion detection methods based on (a) daily means (used in this study) and (b) a fixed reference month (March) in the observations (MERRA2). In (a), the average surface signal is shown for the 30 days after the ozone minimum date, in (b) an average surface signal in March and April is shown for years with ozone depletion. In (a), stippling shows significance at the 4.6% level following a bootstrapping test. In (b), stippling shows significance on a 5% level following a Student's t-test.

S5. Chemical ozone depletion in the models

Figure S10 shows the mixing ratio anomalies of Chlorine monoxide (ClO) around the ozone minima in INT-3D integrations. In both models, there is a positive ClO anomaly around the ozone minima date, which is a strong indication for Chlorine activation. This lends confidence that the ozone minima are largely caused by chemical ozone depletion by ozone depleting substances and justifies the usage of the terms "ozone minima" and "ozone depletion" interchangeably. The magnitude of the ClO anomalies is model-dependent, with SOCOL-MPIOM having a larger ClO abundance than WACCM. This can be traced back to a colder stratosphere and an earlier timing of the ozone depletion in spring in SOCOL-MPIOM and is reflected in the magnitude of the ozone minima (Figs. S3, S8). We note that the amount of ozone depleted cannot be derived solely by ClO concentrations [5], but we deem ClO as a valid qualitative proxy for chemical depletion in our models.

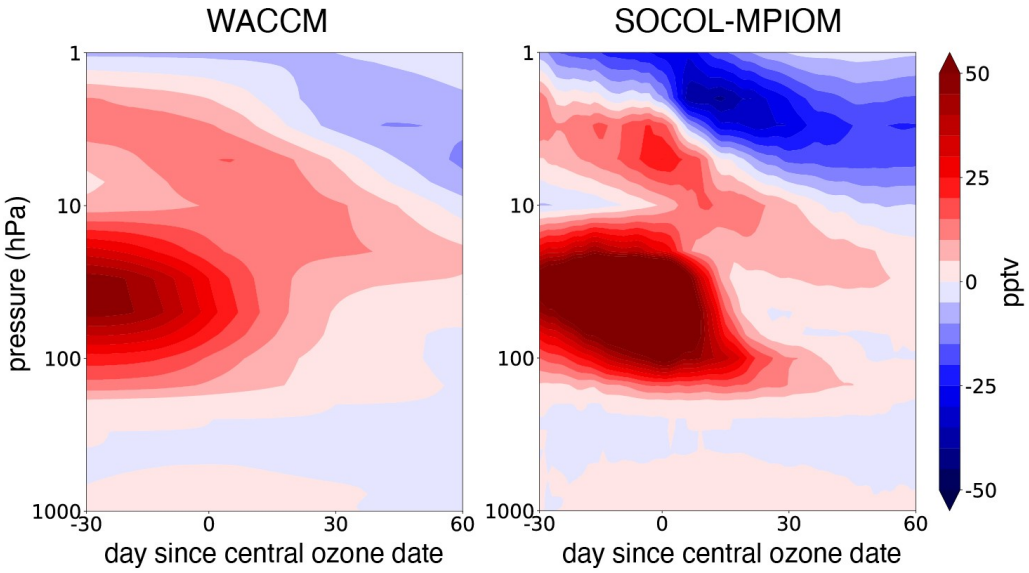

Supplementary Figure S10. Chlorine monoxide as proxy of chemical depletion in the models. Anomalies in ClO mixing ratios around the ozone minimum date in WACCM (a) and SOCOL-MPIOM (b). ClO concentrations in WACCM have been interpolated to daily values from a monthly mean model output. In SOCOL-MPIOM, ClO anomalies are calculated from a daily model output.

References

1. Runde, T., Dameris, M., Garny, H. & Kinnison, D. E. Classification of stratospheric extreme events according to their downward propagation to the troposphere. *Geophys. Res. Lett.* **43**, 6665–6672, DOI: https://doi.org/10.1002/2016GL069569 (2016).
2. Zhang, J. *et al.* The Influence of Zonally Asymmetric Stratospheric Ozone Changes on the Arctic Polar Vortex Shift. *J. Clim.* **33**, 4641 – 4658, DOI: 10.1175/JCLI-D-19-0647.1 (2020).
3. Ivy, D. J., Solomon, S., Calvo, N. & Thompson, D. W. J. Observed connections of Arctic stratospheric ozone extremes to Northern Hemisphere surface climate. *Environ. Res. Lett.* **12**, 024004, DOI: 10.1088/1748-9326/aa57a4 (2017).
4. Calvo, N., Polvani, L. M. & Solomon, S. On the surface impact of Arctic stratospheric ozone extremes. *Environ. Res. Lett.* **10**, 094003, DOI: 10.1088/1748-9326/10/9/094003 (2015).
5. Peter, T. The stratospheric ozone layer—An overview. *Environ. Pollut.* **83**, 69–79, DOI: https://doi.org/10.1016/0269-7491(94)90024-8 (1994).